Aspects of Electromagnetic-Thermal Coupled Optimization of Asynchronous Machines for Traction Drives

J. Buschbeck, M. A. Vogelsberger, A. Orellano, E. Schmidt

Abstract – **The growth of power density in traction motors requires disproportionally more heat to be discharged which leads to the need for more and more advanced cooling techniques. In this paper a novel evaluation and optimization approach for internal air cooled traction machines will be presented. It investigates the electromagnetic performance combined with the aero- and thermodynamic cooling performance. In a first step analytical/ empirical models are used to speed up the calculation time for obtaining pressure drop, volume flow distribution and heat transfer as well as iron stack temperature. The results are validated using computational fluid dynamics simulations of several iron stack cooling duct geometries. Finally, a setup is presented about how the optimization can be implemented coupling electromagnetic losses obtained by finite element analysis with the analytic thermal model.**

Index Terms— **Analytical models, AC motor drives, Design optimization, Induction machines, Thermal management of electronics, Traction motors**

I. Introduction

In comparison to standard industrial variable speed drives, asynchronous induction machines utilized with traction drives always show much higher electromagnetic and thermal utilization. Besides the thermal restrictions, in most cases there are some more conditions defined from the application which strongly influences the design of such machines. Consequently, an optimization with respect to a maximum electromagnetic performance and the thermal limitations must consider fundamental aspects of electromagnetic, thermal and mechanical loadabilities. Additionally, the characteristics of these machines, in particular torque density and stray field inductances, have to be taken into account with the multi-domain optimization.

II. Loadability Aspects

In dependence on the number of pole pairs p, the ratio of stacking length l_i and pole pitch τ_p of induction machines the length ratio χ lies within a typical range of

$$\chi = \frac{l_i}{\tau_p} = (1 \dots 2)\sqrt[3]{p}\,. \tag{1}$$

Therefore, typical lengths of induction machines such as stacking length l_i, air-gap diameter D_i can be assumed to be variable over a length scale λ which means lengths and diameters are proportional to λ [1].

A. Mechanical Loadability

As discussed in [1], the maximum speed of an induction machine becomes inversely proportional to the scale λ,

$$n_{max} \sim \frac{1}{\lambda}\,. \tag{2}$$

Since synchronous rotor speed and stator frequency are proportional, this also holds for the maximum supply frequency.

B. Thermal Loadability

In general, the stationary temperature rise ΔT of an electrical machine caused by any losses P_L follows from

$$\Delta T \sim \frac{P_L}{A_T}\,, \quad A_T \sim \lambda^2\,, \tag{3}$$

where the cooling surface A_T shows a quadratic dependence on the scale λ.

C. Magnetic Loadability

Thereby, magnetic flux density B_δ within the air-gap and supply frequency f determine the hysteresis losses $P_{Fe,Hy}$ and eddy current losses $P_{Fe,EC}$ within the laminated iron as given by

$$P_{Fe,Hy} \sim f\, B_\delta^2\, \lambda^3, \quad P_{Fe,EC} \sim f^2\, B_\delta^2\, \lambda^3\,. \tag{4}$$

With the constant field region, the hysteresis losses are more significant at lower speeds. However, with higher speeds, the eddy current losses will become more interesting. On the other hand, in the field weakening range with $B_\delta\, f \approx \text{const}$, these losses are rather decreasing or constant.

D. Electric Loadability

The power losses of any winding can be written as

$$P_{Cu} \sim J^2\, \lambda^3\,. \tag{5}$$

The temperature rise caused by such losses is directly

This work This work was supported by Bombardier Transportation: PPC/GSC- Drives, Product Development (PDev); CoC Aero- & Thermo-dynamics; REA Region Central, Eastern Europe and CIS.

J. Buschbeck is with Bombardier Transportation, Specialist Engineering Aerodynamics & Thermodynamics, 16761, Hennigsdorf, Germany (e-mail: ext.jan.buschbeck@de.transport.bombardier.com).

M. A. Vogelsberger is with Bombardier Transportation, PPC-Drives Development Center1, 1220, Vienna, Austria (e-mail: markus.vogelsberger@at.transport.bombardier.com).

A. Orellano is with Bombardier Transportation, Vehicle Engineering, Region Central/ Eastern Europe and CIS, 16761, Hennigsdorf, Germany (e-mail: alexander.orellano@de.transport.bombardier.com).

E. Schmidt is with the Institute of Energy Systems and Electrical Drives, Vienna University of Technology, 1040 Vienna, Austria (e-mail: erich.schmidt@tuwien.ac.at).

978-1-4799-4389-0/14/$31.00 ©2014 IEEE

proportional to the product of the RMS value of the current sheet of the armature winding A and the current density J of the winding conductors,

$$\Delta T \sim \frac{P_{Cu}}{A_T} \sim A\,J\,, \tag{6}$$

which is independent of the scale of an electrical machine [1]. Thus, the product $A \cdot J$ is one of the most important design criteria with respect to temperature rise and consequently cooling methods.

E. Torque density

The maximum average tangential stress τ_δ within the air-gap of an induction machine is given by

$$\tau_\delta = \frac{1}{\sqrt{2}} \xi_1\, A\, B_\delta\,, \tag{7}$$

where A denotes the RMS value of the armature current sheet, B_δ the magnitude of the fundamental wave of the radial component of the magnetic flux density within the air-gap and ξ_1 is the total winding factor including pitch, distribution and, if applicable, skewing terms.

The well-known Esson utilization number $C_{IM} = \pi^2\,\tau_\delta$ defines the apparent power S_{IM} of the induction machine in dependence on air-gap diameter D_i, stacking length l_i and synchronous speed n_s as given by

$$S_{IM} = C_{IM}\, D_i^2\, l_i\, n_s\,. \tag{8}$$

On the other hand, the apparent torque T_{IM} of the induction machine follows from

$$T_{IM} = \frac{S_{IM}}{2\,\pi\,n_s} = 2\,\tau_\delta\,V_\delta\,, \tag{9}$$

thus proportional to the product of tangential stress τ_δ and volume

$$V_\delta = \frac{\pi}{4}\, D_i^2\, l_i \sim \lambda^3\,. \tag{10}$$

F. Stray Field Inductances

Typically, the most important portion of the stray field inductances arises from stator and rotor slots. The normalized values of these stray field inductances are proportional to the stray coefficient of the slots λ_σ and can be written as

$$l_\sigma \sim \lambda_\sigma \frac{A}{B_\delta}. \tag{11}$$

Consequently, these inductances depend on current sheet A and air-gap flux density B_δ. It should be mentioned, that the stray coefficient λ_σ is proportional to the ratio of slot height against width.

In order to get a high field weakening capability of the induction machine, the torque characteristic must provide a ratio of the maximum torque to the nominal load torque as the factor of the desired field weakening range. Therefore starting from an initial design which fulfills the criteria of the application, the stray field inductances must not change significantly.

G. Summary

By keeping magnetic as well as electric utilization constant, the losses of an induction machine (4), (5) grow with the third of the scale. However, the cooling surface grows only to the square of the scale. Thus, an increased scale of an electrical machine yields more and more importance for the cooling methods.

Assuming a given temperature rise due to the rather load-independent iron losses, the magnetic flux density can vary in the range of

$$B_\delta \sim \lambda^{0.5} \ldots \lambda\,. \tag{12}$$

As given above, the stray field inductances should be kept constant. Thus,

$$A \sim B_\delta \sim \lambda^{0.5} \ldots \lambda\,. \tag{13}$$

Therefore, the maximum average tangential stress depends on the scale as given by

$$\tau_\delta \sim \lambda \ldots \lambda^2 \tag{14}$$

and the maximum torque T_{IM} of an induction machine (9) grows with the scale as of

$$T_{IM} \sim \lambda^4 \ldots \lambda^5\,. \tag{15}$$

However, an increasing armature current sheet A asks for a decreasing current density J within the windings. But the stray field inductances restricts rather to a constant current density. Consequently as given by (6), the cooling of the load-dependent losses asks for efficient cooling methods additionally.

III. Temperature Distribution

To model the temperature distribution within the machine, the 1D temperature field equation can be solved with given heat source terms. When heat source per volume $\dot{W}$ and thermal conductivity k are assumed to be piecewise constant, the temperature field can be described with

$$T(r) = -\frac{\dot{W} r^2}{4\,k} + c_a + c_b \ln\frac{r}{r_0}, \tag{16}$$

where c_a and c_b are constants to be defined by boundary conditions. In the center symmetry condition is applied, between parts no isolation is present, thus no step change in temperature occurs and housing temperature must be defined. Fig. 1 shows the resulting temperature distribution with temperature differences to housing temperature (ΔT). The air-gap is modeled as heat conducting only thus heat transfer through convection is assumed not to be present.

This results in an overestimated thermal insulation between stator and rotor. However, in the presented case no heat is transferred through the air-gap due to equal sink and source terms in stator and rotor, respectively.

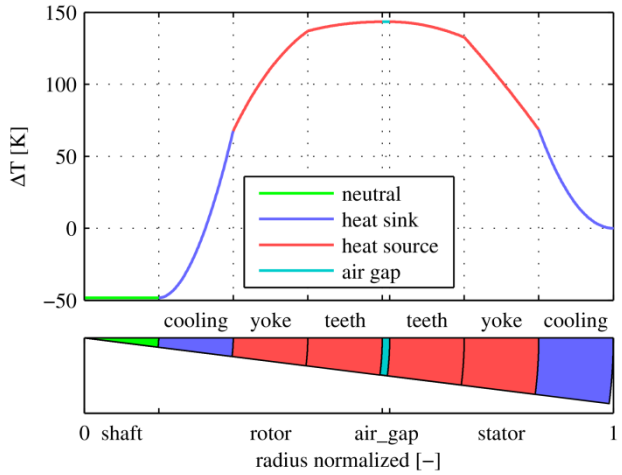

Fig. 1. Temperature distribution (ΔT temperature differences to housing temperature); 1D model (top), visualization of sink/source locations in the stacking cross section (bottom).

A bend in curve shape occurs on joints between parts due to changing conductances. Heat source and sink terms are equal, thus no heat is exchanged through the housing which is equivalent to no present temperature gradient to the outside.

The model overestimates temperature change due to no heat exchange through the front and back sides. The magnified thermal insulation of the air-gap leads to higher temperature differences between stator and rotor if the sink/ source terms do not equal out. However, from this general observation it can be concluded that a positive net heat flux in the rotor should drastically be avoided.

IV. Optimization Strategy

Different cooling duct configurations are investigated where the flow is directed axially and cooling fluid passes through stator and rotor. Cooling ducts can be placed in iron yoke areas, see Fig. 2 (blue and red labeled areas)

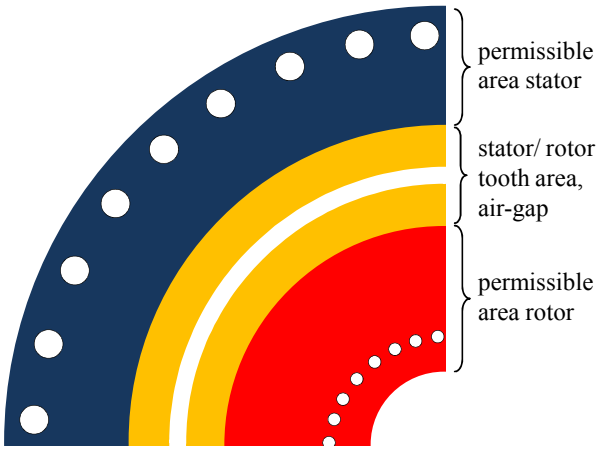

Fig. 2. Permissible area for cooling ducts, example duct geometries.

The optimization evaluates both the electromagnetic performance as well as the temperature level needed for the heat removal. The two evaluations are one way coupled, within the electromagnetic calculation the heat sources for the thermal model are determined.

Fig. 3 shows the optimization loop. Each step is described in the following subsections.

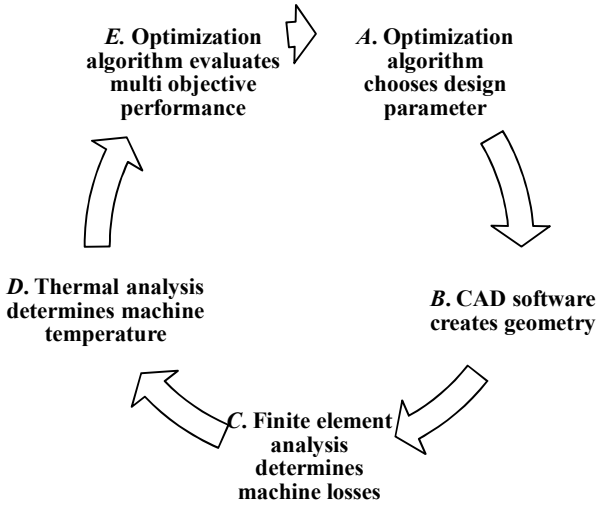

Fig. 3. Optimization loop.

A. Parameters

The parameters of the cooling duct geometry are listed in Table 1. The indices *'r'* and *'s'* denote the parameter for rotor and stator, respectively. The prefixed *'f'* for function of the parameter name marks the difference to the actual geometric quantity. In total there are 14 parameters describing 14 geometric quantities. The geometric parameters are 'position', describing the radial distance from the center point, 'a' defining the length of the upper edge, 'b' defining the ducts height, 'c' defining the length of the bottom edge and '*r_a'* and '*r_c'* defining the radius of the vertices of the edges 'a' and 'c', respectively. The remaining parameters describe fluid mechanical properties which determine the remaining geometric quantities to fully describe the ducts geometry with using the analytic model for pressure drop described in V. *'f_rotor_stator'* defines the mass flow distribution between rotor and stator and *'p_target'* defines the target pressure to determine the number of ducts in rotor and stator, each.

TABLE 1
PARAMETERS CONVERSION WITH RANGES

Parameter	Geometric quantity	Parameter range	Geometric range
f_position_r,s	position_r,s	[0, 1]	[R_min, R_max]
a_r,s		[0.001, 0.2]	
f_b_r,s	b_r,s	[0, 1]	[≈0, b_max]
f_c_r,s	c_r,s	[0, 2]	[0, 2a_r,s]
f_r_a_r,s	r_a_r,s	[0, 1]	[0, r_a_max]
f_r_c_r,s	r_c_r,s	[0, 1]	[0, r_c_max]
f_rotor_stator	no_ducts_r,s	[0, 1]	[2, ∞]
p_target		[0, 1559.5]	

The workflow is structured in three parts: First, the shape of the ducts is constructed converting the parameters to geometric quantities. Next, the area and circumference of the ducts are calculated. Then, the duct numbers can be obtained in such a way to fulfill the pressure and flow distribution constraints. Analytical formulae are used to calculate iron stack temperature which is presented in section V.

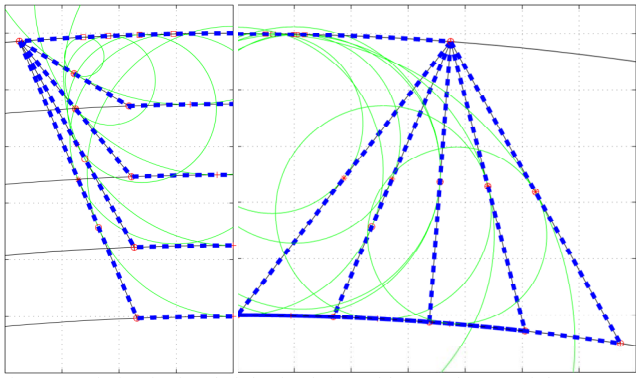

Fig. 4. Variation in duct height 'b' (left) and lower edge 'c' (right).

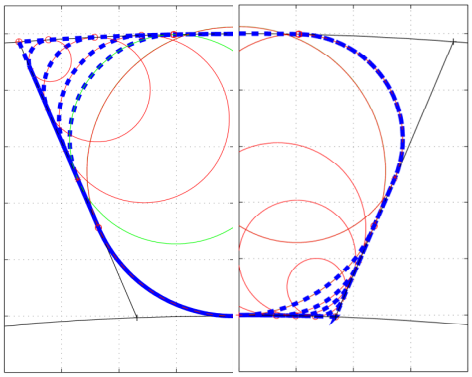

Fig. 5. Variation in upper radius 'r_a' (left) and lower radius 'r_c' (right).

B. *Geometry Creation*

The CAD software is able to allocate every design input to a parameter. After geometry creation, a 2D geometry is exported for the finite element analysis whereas the computational fluid dynamics (CFD) needs the full 3D model.

C. *Electromagnetic Evaluation*

The electromagnetic evaluation is automated by a script driven finite element analysis.

Preprocessing: First, the geometry is imported and the predefined mesh settings are applied, physic quantity definitions like material properties, supply voltage sources, etc. are loaded.

Solving: Two cases are calculated. To obtain magnetizing current and average flux densities in tooth and yoke region no load state is simulated. In a second run, the load case defines iron losses as well as resistive losses.

Open source MUMPS[1] is used, a direct solver capable of utilizing parallelization. The advantage here is that the solver can allocate its own memory in addition to reserved memory by the software [2]. Then, solving parameters like precision, iteration number and relaxation factor are defined and the two solving scenarios 'load case' and 'no load case' are set up.

Postprocessing: After performed calculation the needed output values are computed. To consider additional losses e.g. due to the deterioration of the sheet permeability after the stamping process, Bombardier Transportation's internal equations for loss prediction are used to obtain values closer to measurements performed before.

[1] Stands for Multifrontal Massively Parallel sparse direct Solver, see http://mumps.enseeiht.fr.

D. *Thermal Analysis*

The thermal analysis is performed analytically. The core element is to obtain the heat transfer coefficient with an empirical approach to calculate the Nusselt number. Then, the surface temperature is iterated until discharged energy equals the loss heat source terms, thus the steady state is reached. The analytical model used is described in the next section.

E. *Optimization Algorithm*

Optimization algorithms must choose designs in a way the (pareto) optimum is reached with minimal design evaluations required. The group of evolutionary algorithms mimic the natural selection process for this purpose. In this analogy, a single gene is equivalent to a parameter, a chromosome to one design and the design space is equivalent to the whole population. To create new designs the following mechanisms can be applied [3]: Crossover interchanges sections of the chromosomes of parent designs with a certain probability. Mutation modifies single genes, the mutation ration defines hereby the percentage of modified genes. Selection and elitism ensures the preservation of best designs in the population [4]. The Multi-Objective Genetic Algorithm (MOGA-II) is used.

V. Analytic Model

Analytical formulae are used to cover pressure loss calculation as well as iron stack temperature determination. All used formulae and coefficients for pressure and heat transfer are given in [5]. Pressure loss of a single duct is calculated

$$\Delta p = \sum \zeta_i \cdot \frac{\rho\, v^2}{2}, \tag{17}$$

with ζ_i being a pressure drop coefficient for tube, inflow and outflow, v is the mean flow velocity and ρ the density. For the tube pressure drop coefficient ζ_{tube} formula from Hermann (18) is used valid in present Reynolds number range ($2300 < \mathrm{Re} < 2 \cdot 10^6$)

$$\zeta_{tube} = \left(0.00540 + \frac{0.3964}{\mathrm{Re}^{0.3}}\right) \frac{l}{d}, \tag{18}$$

with duct length l and duct diameter d. [5] gives for inflow pressure drop coefficients with sharp edges $\zeta_{inflow} = 0.5$. Caused by the relative movement of the rotor the flow enters the rotor ducts with an angle δ. With (19) the coefficient increase can be approximated to $\zeta_{inflow,rotor} \approx 0.75$.

$$\zeta_{inflow,rotor} = 0.3 \cos\delta + 0.2 \cos^2\delta \tag{19}$$

On the outlet the flow experiences a drastic change in cross section area A_1/A_2 leading to the pressure drop coefficient

$$\zeta_{outflow} = \left(1 - \frac{A_1}{A_2}\right)^2. \tag{20}$$

In a parallel configuration of tubes the pressure drop

before inlet and after outlet must be equal. A script iterates the volume flow distribution and therefore the mean velocities in the ducts in such a way to utilize the same pressure drop. Non circular duct cross sections are covered using the common *hydraulic diameter* which is derived using the shear stress approach.

The heat transfer is modeled with an empirical formula for the Nusselt number which is describing the ratio between convection and conduction heat transfer. Equation (24) is valid for flow states with Reynolds numbers between $10^4 \leq \mathrm{Re} \leq 10^6$ and Prandtl numbers in the range of $0.6 \leq \mathrm{Pr} \leq 1000$. Equation (21) describes heat transfer per surface $\dot{q}$ with logarithmic temperature $\Delta T_{\ln}$ given in (22) where T_W is the wall temperature, T_{in} and T_{out} the in- and outflow temperature, respectively.

$$\dot{q} = \alpha \, \Delta T_{ln} \tag{21}$$

$$\Delta T_{ln} = \frac{(T_W - T_{in}) - (T_W - T_{out})}{\ln\left(\frac{T_W - T_{in}}{T_W - T_{out}}\right)} \tag{22}$$

The heat transfer coefficient α needs to be determined with the Nusselt number given in (24)

$$\alpha = \frac{\mathrm{Nu}\, k}{d}. \tag{23}$$

$$\mathrm{Nu} = \frac{(\xi/8)\mathrm{Re}\,\mathrm{Pr}}{1 + 12.7\sqrt{\frac{\xi}{8}}\,(\mathrm{Pr}^{\frac{2}{3}} - 1)}\, f_1\, f_2\,, \tag{24}$$

where ξ is the tube friction number

$$\xi = (1.8 \log \mathrm{Re} - 1.5)^{-2} \tag{25}$$

and factor f_1 considers growing boundary thickness along the tube and f_2 factors in heat flux direction.

$$f_1 = 1 + \left(\frac{d}{l}\right)^{2/3} \tag{26}$$

$$f_2 = \left(\frac{T}{T_{Wall}}\right)^{0.45} \tag{27}$$

VI. Analysis Results

The results of the validation using CFD simulations show the applicability of the analytical formulae for optimization purpose. For single duct geometry with circular and squared cross section the pressure drop and heat transfer was within an accuracy of 2.2 % varying the mean velocity between 5 and 22 m/s. However, several parallel duct settings are calculated as well with imprinted rotation of the rotor ducts. CFD code (CD-adapco's StarCCM+ Version 8.02.008) with conjugate heat transfer, *kω*-turbulenz model and segregated flow was used. Comparison between CFD results and analytical tool are shown in Fig. 6 and Fig. 7.

Results from CFD and analytical tool match very well. The pressure loss is predicted very accurately, however the last three designs (*g, h, i*) do deviate up to 15 % because of geometries with extreme width to height ratios (up to 1 to 7.5).

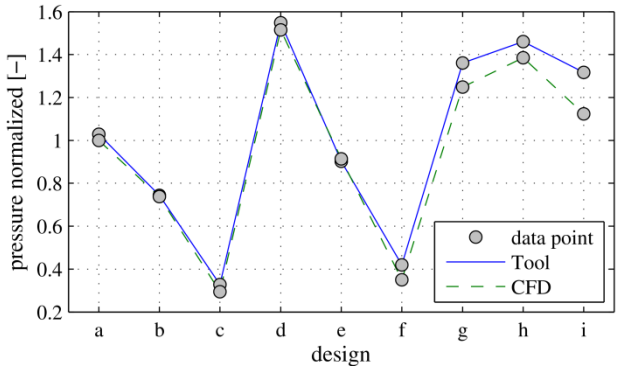

Fig. 6. Pressure validation.

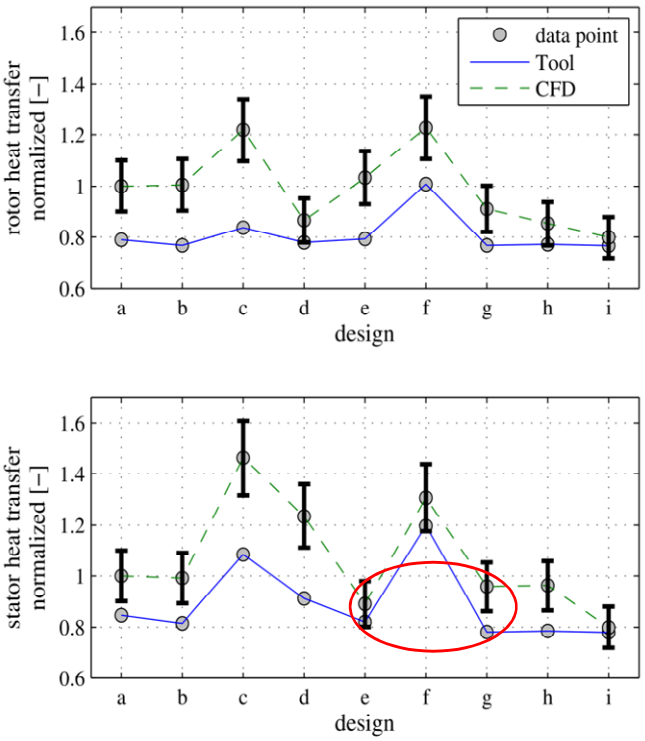

Fig. 7. Heat transfer validation, top rotor, bottom stator.

Most important for optimization purpose is that the trend is covered correctly which is the case for all designs calculated. As ideal design for cooling ducts, elongated hole shape was found out.

The heat transfer in CFD simulations varies strongly with used turbulence model and mesh settings. Based on this, the error is approximated of about 10 % which is visualized by the error bars. Heat transfer is underestimated by the analytical tool but the trend is covered in most cases. Comparing the stator heat transfer of design *e* and *g* shows a violation of the trend. Analytics determine higher heat transfer for design *e* compared to *g* whereas CFD calculated it lower than for design *g*. However, the difference is within the error margin.

VII. Conclusion

Results show that analytical formulae can be used to model pressure drop, volume flow distribution and heat transfer for optimization purpose. The validation of the

model with CFD showed that the pressure drop is predicted very accurately for round geometries whether geometries with large width to height ratio deviate more. However, the trend is covered correctly which is the crucial aspect for optimization. Good coverage of the trend for heat transfer could also be proved because it lay inside the approximated error margin of the CFD. Moreover, the introduced optimization setup shows the implementation of coupled electromagnetic and thermal design evaluation.

REFERENCES

[1] J. Pyrhönen, T. Jokinen, and V. Hrabovcová, *Design of Rotating Electrical Machines*. John Wiley & Sons Ltd, 2008.

[2] CEDRAT, "User Guide Flux 11," Manual Réf. K101-111-EN-07/12, .2

[3] N. Gould, *An Introduction to Angorithms for Countinuous Optimization*. Laboratory, Oxford University Computiong Laboratory and Rutherford Appleton, 2006.

[4] C. R. Reeves and J. E. Rowe, "Genetic Algorithms - Principles and Perspectives: A Guide to GA Theory," *Operation Research/ Computer Science Interfaces Series*, vol. 20, 2003.

[5] VDI-Gesellschaft Verfahrenstechnik, *VDI Heat Atlas*, 2nd ed., V. D. Ingenieure, Ed. Berlin: Springer, 2010.

BIOGRAPHIES

Jan Buschbeck received the B.Sc. in Physical Engineering with specialization in fluid mechanics from Berlin University of Technology, Germany in 2012. He is enrolled in the M.Sc. Physical Engineering program with specialization in fluid mechanics and acoustics. He has been working for Bombardier Transportation CoC Aero- and Thermodynamics, Hennigsdorf, Germany since 2011 as a student. There, he coordinates the R&D-Project “Thermo efficient traction motor design”. His master thesis is realized as a cooperation between Berlin University of Technology Fluid Dynamic department, Vienna University of Technology Electrical Drives department and Bombardier Transportation and contributes to the R&D-Project.

Markus A. Vogelsberger received the the Dipl.-Ing./M.Sc. (with honor) and Dr.Techn/Ph.D. (with honor) degrees in Electrical Engineering from Vienna University of Technology, Vienna, Austria, in 2004 and 2009, respectively. He has been a scientific sesearch assistant at the Institute of Electrical Drives and Machines, Vienna University of Technology, where he has been engaged in several industrial and scientific R&D projects in the field of sensorless control, drives systems and power electronics / drive converter and interdisciplinary topics. He received awards and scholarships from Austria Goverment for excellent research and study performance in 2005 & 2006 respectively. He joint Georgia Institute of Technology University, Atlanta/USA for study and international research activities for several months in 2006 and 2008, respectively.
In 2011, he joined Bombardier Transportation, Vienna, Austria, as a Development Engineer and R&D Project lead in the PPC-Drives Department. His field of interest include power electronics, simulation of electrical drives, motor design as well as high innovative multidisciplinary R&D-Projects. In particular, currently his focus as responsible R&D-Project Lead for Drives is on the research/development and managing of the high inovative condition monitoring strategy (OIM) for ac traction drives and on the interdisciplinary R&D-Project - thermo efficient traction motor design. design.

Alexander Orellano received his diploma degree in Aerospoace Engineering 1993 at the University of Technology in Munich. He worked at the University of the German Armed Forces as researcher starting 1993 where he was responsible for a DFG (Deutsche Forschungsgemeinschaft) funded research program related to the control of turbulence. Alexander received his degree as Dr.-Ing./Ph.D. (Summa cum Laude) in Aerodynamics 2000. He worked two years as consultant for the automotive industry in the field of aeroacoustics. He started his career in the rail business in 2000 entering ADtranz (later Bombardier). He was responsible for the Center of Competence for Aerodynamics and Thermodynamics until 2012 working successfully in developing the ZEFIRO high speed train family of Bombardier. Today he is heading the Vehicle Engineering function in the Region Central and Eastern Europe and CIS of Bombardier. In this function he is responsible for the concept, the architecture and product management of high-speed, regional, commuter and metro trains.

Erich Schmidt was born in Vienna, Austria, in 1959. He received his M.Sc. and Ph.D. degrees (with honor) in Electrical Engineering from the Vienna University of Technology, Austria, in 1985 and 1993, respectively. Currently, he is an Associate Professor of Electrical Machines at the Institute of Energy Systems and Electric Drives of the Vienna University of Technology. His research and teaching activities are on numerical field computation techniques and design optimization of electrical machines and transformers. He has authored more than 100 technical publications mainly in the fields of electrical machines and numerical field calculation.